

X-Ray Computed Microtomography Studies of Fluid Partitioning in Drainage and Imbibition Before and After Gel Placement: Disproportionate Permeability Reduction

R.S. Seright, SPE, New Mexico Petroleum Recovery Research Center, and Masa Prodanovic and W. Brent Lindquist, SPE, Stony Brook U.

Summary

X-ray computed microtomography (XMT) was used to establish why pore-filling Cr(III)-acetate-HPAM gels reduced permeability to water much more than to oil. Our results suggest that permeability to water was reduced to low values because water must flow through gel itself, whereas oil pressing on the gel in Berea sandstone or porous polyethylene forced pathways by dehydration—leading to relatively high permeability to oil. In very permeable sandpacks, data from other researchers support ripping or extrusion mechanisms for creating oil pathways.

Our XMT studies provide interesting insights into imbibition and drainage processes in water-wet and oil-wet porous media even before gel placement. Many of our observations were consistent with conventional wisdom. However, some were unexpected. Residual wetting-phase (water) saturations in Berea were surprisingly low-valued in small pores. We attribute this to surface roughness caused by clay coating on Berea's pore walls, which allowed efficient water drainage from small pores during oil injection.

Introduction

Gels have often been injected into production wells in an effort to reduce water production without seriously damaging hydrocarbon productivity. To be effective, the gels must significantly reduce permeability to water while causing minimal reduction in permeability to oil. Many gels exhibit this disproportionate permeability reduction, but the property has not been as predictable as we would like. If the mechanism for this property were understood, gel treatments could be applied with greater reliability. To determine this mechanism for a Cr(III)-acetate-HPAM gel, we used XMT. As an important prelude to investigating gel behavior in porous media, XMT was used to characterize imbibition and drainage processes in water-wet and oil-wet porous media before gel placement.

Fluids, Cores, and Flooding Procedures

The aqueous Cr(III)-acetate-HPAM gel used in this work contained 0.5% Alcoflood 935 HPAM ($\sim 5 \times 10^6$ daltons, 5 to 10% degree of hydrolysis), 0.0417% Cr(III) acetate, 1% NaCl, and 0.1% CaCl₂. The brine contained 1% NaCl and 0.1% CaCl₂. The oil was hexadecane that was doped with either 10% iodoheptadecane (used in Berea) or 15% bromohexadecane (used in polyethylene) to increase X-ray attenuation contrast relative to the brine phase. All experiments were performed at room temperature, except after gelant injection, when the core was heated to $\sim 60^\circ\text{C}$ for 12 hours to induce gelation.

Wettability tests produced Amott-Harvey indices (Boneau and Clampitt 1977) of 0.7 for the brine/oil/Berea sandstone system and

~ 0.8 for the brine/oil/porous polyethylene system, confirming the water-wet character of Berea sandstone and the oil-wet character of porous polyethylene.

The 6.5-mm-diameter, 3-cm-long cores were coated with a thin layer of epoxy and mounted with inlet and outlet fittings that allowed flooding between image acquisitions. The Berea core [specifically, the "first Berea core" discussed in Seright et al. (2002), Seright (2003a), and Seright et al. (2004)] had a permeability of 0.47 darcys and a porosity of 22%. The polyethylene core had a permeability of 8.8 darcys and a porosity of 40%. Each core was initially saturated with wetting fluid (brine for Berea, oil for polyethylene). A vacuum was first applied to each core to ensure saturation. Subsequently, each core was subjected to drainage and imbibition displacements as listed in **Table 1**.

All displacements were continued until residual conditions for the displaced fluid were achieved. Achievement of residual conditions was verified by monitoring the pressure drop and flow rate as the injection proceeded. The polyethylene core was subjected to two drainage displacements to bring it to residual oil before gelant injection. Gel placement was followed by a drainage/imbibition cycle to re-establish S_{wr} and S_{or} conditions for computation of water and oil residual resistance factors. Residual resistance factors for a given phase (F_{rro} for oil, F_{rrw} for water) were determined by dividing the phase steady-state mobility before gel placement by the phase steady-state mobility after gel placement. XMT images were obtained after each flood. All floods and imaging were performed without removing the core from its mount on the imaging stage. Consequently, saturation changes were followed for individual pores throughout the flooding sequences.

Oil and water injection were performed at constant pressure gradients of 173 psi/ft in Berea and 35 psi/ft in polyethylene. Capillary numbers were approximately 6×10^{-5} in Berea and 2×10^{-4} in polyethylene. These capillary numbers are above the normal range for field-scale waterfloods and above the range where the residual nonwetting-phase saturation is independent of capillary number. Lower capillary numbers would be preferred; our experimental choices were dictated by time limitations associated with the tomography procedures. Gelant injection occurred at 17 psi/ft in Berea and 23 psi/ft in polyethylene. At the flow rates used, the gelant solutions exhibited effective viscosities that were insensitive to fluid velocity.

Descriptions of ExxonMobil's X2B tomographic imaging facility at Brookhaven Natl. Laboratory are provided in Dunsmuir et al. (1991), Flannery et al. (1987), and Seright et al. (2003). To avoid end effects, imaging was performed within a 6.5-mm-diameter, 3.25-mm-long segment of each core centrally located along its 30-mm length. Voxel resolution was $4.1 \mu\text{m}$ for the polyethylene core. The total imaged volume was 29.06 mm^3 , but image analysis on a workstation with 1 Gbyte RAM restricted analysis to a $450 \times 450 \times 475$ voxel (6.63 mm^3) region of each image. For Berea, the resolution was $4.93 \mu\text{m}$, the imaged volume was 50.52 mm^3 , and the volume analyzed was 11.53 mm^3 ($450 \times 450 \times 475$ voxels).

Copyright © 2006 Society of Petroleum Engineers

This paper (SPE 89393) was first presented at the 2004 SPE Symposium on Improved Oil Recovery, Tulsa, 17–21 April, and revised for publication. Original manuscript received for review 12 January 2004. Revised manuscript received 1 August 2005. Paper peer approved 7 September 2005.

TABLE 1—DISPLACEMENT SEQUENCE FOR EACH CORE						
Injected fluid	brine	oil	brine	gelant	oil	brine
Saturation condition	S_{or}	S_{wr}	S_{or}	S_{or}	S_{wr}	S_{or}
Core/initial fluid						
Berea/brine		D	I	G	D	I
Polyethylene/oil	D	I	D	G	I	D

D: drainage; I: imbibition; G: gelant injection

Image Analysis

Fig. 1 shows a small region from each core image throughout the injection sequence. Differentiation of X-ray attenuation coefficient values for grain, oil, and water phases is visually evident. In Berea, the grain phase has the greatest attenuation (darkest phase in Fig. 1); in polyethylene, the grain phase is the least attenuating. Fig. 2 shows the attenuation coefficient distribution in the void space of the imaged region in the Berea core throughout the injection sequence. The (lower-attenuating) water- and (higher-attenuating) oil-phase peaks are clearly visible in the distribution. Superimposed on this plot is the attenuation coefficient distribution for the entire water-saturated image. As the core has porosity of 22%, this latter distribution is dominated by the broad grain-phase peak. Because the grain phase in Berea has highly attenuating impurities, the grain peak tends to be broader than that for the liquid phases. For brevity, we do not show the similar histograms for the polyethylene data; the results are analogous.

The 3DMA-Rock (Lindquist et al. 1996; Lindquist and Venkatarangan 1999; Lindquist et al. 2000, Lindquist website) software package was used to analyze the image sequences. Its segmentation algorithm, based upon indicator kriging (Oh and Lindquist 1999), was used to segregate grain/void space in the first image in each sequence, and to separate oil/water phases within the pore space in each subsequent image. Our segmentation results, corresponding to the regions shown in Fig. 1, are shown in Fig. 3. As shown in Oh and Lindquist (1999), this technique is far superior to global thresholding techniques and produces smooth phase

interfaces. We used indicator kriging segmentation directly on the void-space regions of the tomographic image rather than global thresholding on subtracted images. This produces segmented results superior to our earlier work. [Contrast Fig. 3 with Figs. 10 and 11 in Seright et al. (2002).] Further comparisons with our earlier work can be found in Seright (2003a) and Seright et al. (2004).

As phase segmentation is central to this work, it is important to address phase-identification error. Oh and Lindquist (1999) provide a detailed study of error rates for the indicator kriging algorithm in segmenting two-phase images. The additional complication in this study is the presence of a third phase. In each image, the grain phase has an attenuation coefficient distribution that overlaps strongly with the nonwetting-fluid phase. The grain phase is therefore identified in the first (wetting-phase-saturated) image in each sequence (Fig. 3). The accuracy of its identification in subsequent images depends on precise voxel alignment. The reproducibility precision in the rotation and translation stepping motor [Klinger™ (Newport)] controlling the sample mounting stage on X2B was 0.01° and $0.1 \mu\text{m}$, well below voxel resolution. However, translations of the core throughout an image sequence were observed, the largest of which were observed in the gel image. During the heating period to induce gelation, some movement probably occurred because of sample expansion and softening of the epoxy that cemented the sample in place. This translation was larger for the polyethylene sample than for the Berea core. Smaller translational movements between images were seen before and after gel placement. These may be induced by stress placed on the cementing epoxy when pumping pressure was cycled on and off during fluid injection before imaging the core. Translations were corrected manually using small impurity features in the sample to guide realignment. (Small air bubbles in the grain phase were used in the polyethylene sample—one is visible in Fig. 1 in the upper left-hand grain. Edges of small, highly attenuating impurities in grains were used in the Berea sample—none of these are visible in Fig. 1.) All images were realigned to the first image in the sequence. We assess that the realignment is accurate to within a voxel. The major implication for this is a possible grain-for-nonwetting-phase misidentification within a 1-voxel layer of the surface in a pore. This would result in an overprediction of non-

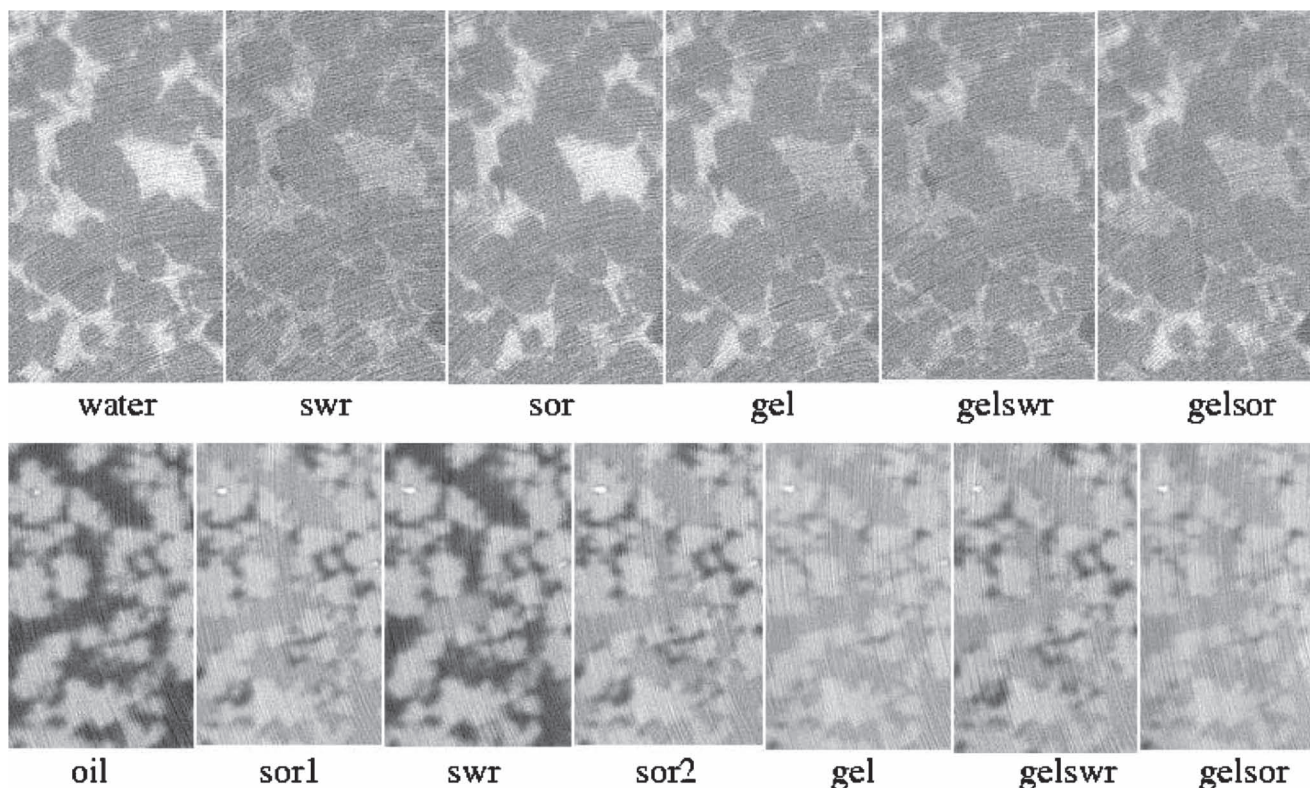


Fig. 1—Tomographic images of a region in the Berea (top) and polyethylene (bottom) cores through the injection sequence.

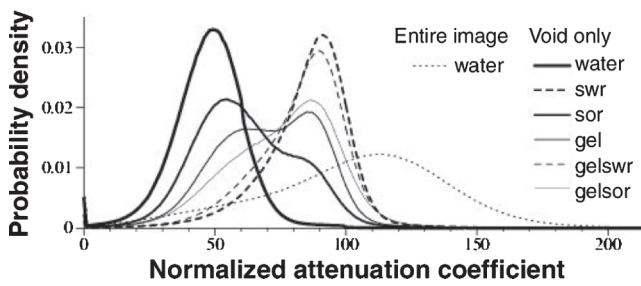


Fig. 2—Attenuation coefficient distributions in the void space of the imaged region in the Berea core throughout the injection sequence.

wetting phase along roughly one-half of the pore surface and loss of fluid identification along the remaining half. Thus, alignment errors can result in the overprediction of the nonwetting phase and can mimic nonwetting-phase films. The bound on this error is roughly the surface-to-volume ratio of the void space. Any alignment errors plus a voxel resolution of several μm make us cautious of any claims for viewing thin films under present XMT capabilities.

Table 2 summarizes the overall water saturations obtained in the analyzed region after each flooding step.

The other major algorithms from 3DMA-Rock used in this analysis are throat-finding algorithms that, using a modified medial axis of the void space as a searchable network, locate local minima in cross-sectional area. With throat surfaces established, a pore-throat network model of the imaged region can be reconstructed. It is important to note that the entire void-space volume is partitioned among pore bodies. The throats themselves are triangulated surfaces of zero volume. These algorithms are also used in analyzing fluid-blob aspect ratios. In the interests of brevity, we refer the reader to Lindquist and Venkatarangan (1999), Lindquist et al. (2000), Shin et al. (2005), and Prodanovic et al. (in process) for in-depth discussions of these pore-throat partitioning algorithms.

Fig. 4 compares the pore-size distributions for Berea sandstone and porous polyethylene. The analyses examined 2,176 pores for the Berea sample and 1,879 pores for the polyethylene sample. The average pore size for polyethylene (0.00052 mm^3) was 44% greater than that for Berea (0.00035 mm^3). Interestingly, the median pore size was greater for Berea (0.00016 mm^3) than for polyethylene (0.00010 mm^3). The higher average for polyethylene occurred because it contained a larger fraction of pores with sizes greater than 0.002 mm^3 (compare the high end of the distributions in Fig. 4). Incidentally, if the pores were spherical (which they are not), the average pore radius would be $50 \mu\text{m}$ for polyethylene and $44 \mu\text{m}$ for Berea. For each flooding stage, the fluid-phase saturations vs. pore size were compared.

Identification of individual fluid blobs and connectivity of these blobs was done using a standard grassfire algorithm (Pitas 1993). The voxels of the two fluid phases must be treated with different connectivity by such algorithms in order to preserve logical consistency of surface boundaries. We consistently used 26-connectivity for voxels of the wetting phase and 6-connectivity for the nonwetting phase. (Flipping this choice produces minor changes in the blob statistics reported here.)

Fig. 5 uses the ability to identify single pores and fluid blobs to examine changing fluid occupation within a single Berea pore. The grain surface of the pore is shown as a (partially transparent) gray mesh surface. The pore has coordination number 4, and the view into the pore is through one channel entrance. The red blobs show the position of oil within the pore at residual oil conditions (S_{or} before gel). The green blobs show the position of water in the pore at residual water conditions (S_{wr} before gel). The positioning of the blobs in this pore follows conventional wisdom, with the residual oil residing more in the pore center and residual water lying along the pore surface.

Imbibition and Drainage Before Gel Placement

Comparison between drainage and imbibition in both porous media before gel placement provided an interesting insight into conventional wisdom.

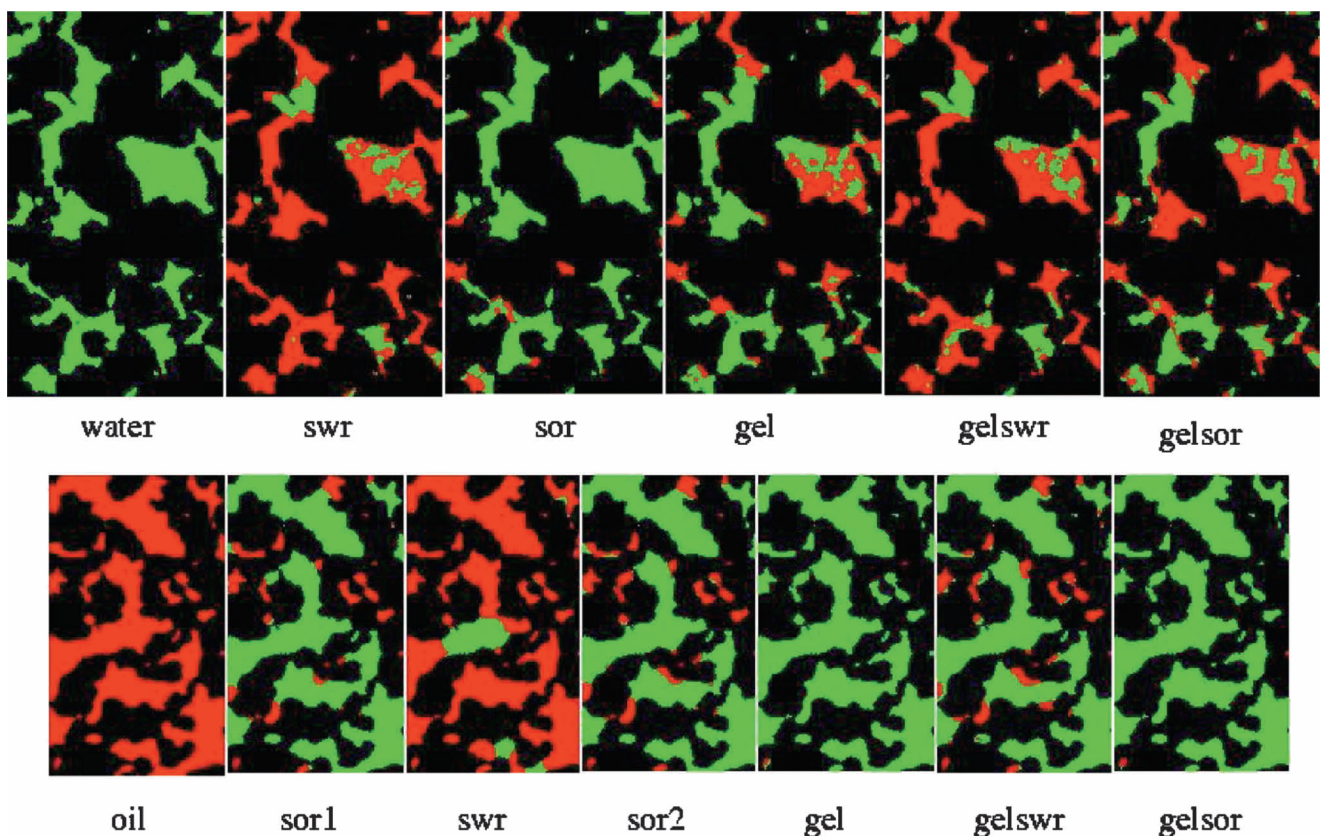


Fig. 3—Segmented images of the region in Fig. 1. Oil=red; water=green; grain=black.

TABLE 2—WATER SATURATION AFTER VARIOUS FLOODS

	Berea	Polyethylene
At S_{or1} before gel		86.0%
At S_{wr} before gel	16.0%	16.5%
At S_{or} or S_{or2}	81.6%	83.0%
At Gel placement	63.7%	99.8%
At S_{wr} after gel	28.7%	83.5%
At S_{or} after gel	49.0%	99.7%

Oil Drainage From Oil-Wet Polyethylene: S_w Values Were Consistent With Conventional Wisdom. When a wetting phase drains from a porous medium, conventional wisdom argues that the smallest pores should retain the highest wetting-phase saturation. This expectation is consistent with our findings after water injection into (oil drainage from) oil-wet porous polyethylene (Fig. 6). After the first drainage displacement (S_{or1}), oil saturation in the imaged region of the polyethylene core was 14%. Oil saturations at S_{or} are plotted in Fig. 6 for each of the 1,879 pores in this region. The solid curve plots the average oil saturation as a function of pore size. As expected, the average oil (wetting-phase) saturation in the smallest detected pores was more than 80% (Fig. 6), while the medium-to-large pores were more likely to be filled with water.

During a second cycle of oil drainage (i.e., a second waterflood to drive the core to S_{or2} after an intervening oil flood), most large pores again filled almost completely with water, while most small pores retained high oil saturations (Fig. 7).

Oil Imbibition Into Polyethylene: Oil Was Immobile in Small Polyethylene Pores. As mentioned, at S_{or} , most small pores had nearly 100% oil saturation, while most large pores had nearly 100% water saturation (Fig. 6). When oil was injected to drive the core to S_{wr} (Fig. 8), water was displaced from most medium-to-large pores so that most pores ended with nearly 100% oil saturation. Thus, consistent with conventional wisdom, the wetting phase was largely immobile in small polyethylene pores.

Water Drainage From Berea: The Saturation Distribution Deviated From Conventional Wisdom. In Berea sandstone, at connate water saturation (S_{wr}) before gel placement, S_w in the imaged region was 16%. The water saturations at S_{wr} are plotted in Fig. 9 for each of the 2,176 pores in Berea. The solid curve plots the average water saturation as a function of pore size. At S_{wr} , 54.5% of the pores had $S_w < 5\%$; water saturations near zero were com-

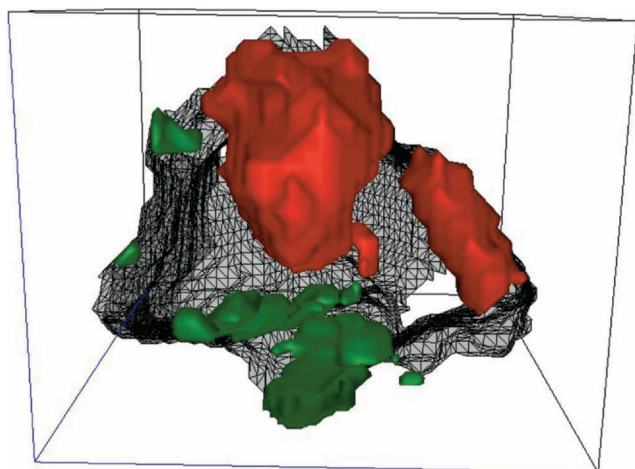


Fig. 5—Measured positioning of residual fluid phases [oil at S_{or} (red) and water at S_{wr} (green)] tends to follow conventional wisdom in this Berea pore.

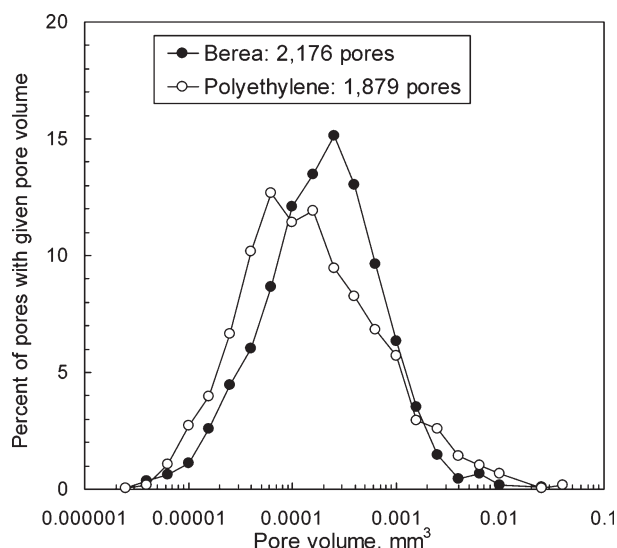


Fig. 4—Pore-size distributions for Berea and polyethylene.

mon for pores in most size ranges. The solid curve suggests that the average water saturation in the smallest detected pores was less than 60%. However, few pores existed at the small end of the distribution, so an average value may not be particularly representative. Even so, it is clear that water saturations in the smallest pores were scattered over the entire range from 0 to 100%—just as in most other size ranges.

On first consideration, this finding appears to contradict the expectation that the water saturations approach 100% in the smallest pores of a water-wet porous medium. The work of Dullien et al. (1989) helps to explain the behavior that we see in Berea and why it deviates from that in polyethylene. Berea pores are typically coated with kaolinite that significantly increases the surface roughness of the pore walls. In contrast, the pore walls in polyethylene are quite smooth. [Scanning electron microscope images of the two samples are shown in Seright et al. (2002), Figs. 3 and 4.] At S_{or} , after oil drainage from the smooth polyethylene pore walls, an extremely thin (nanometer-scale) oil film may have coated most pore walls (or possibly, no film may remain). At S_{wr} in water-wet Berea, the rough clay coating made the effective thickness of the water film much greater than for any oil film in porous polyethylene. With a thicker effective wetting film, water drained fairly efficiently from the smallest detected Berea pores when oil was injected, thus allowing the smallest detected pores to reach water saturations comparable to those in larger pores (Fig. 9). In contrast,

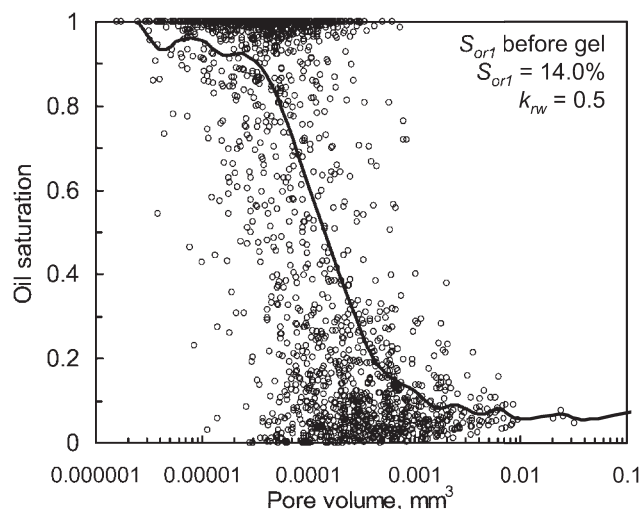


Fig. 6—Polyethylene at S_{or1} before gel.

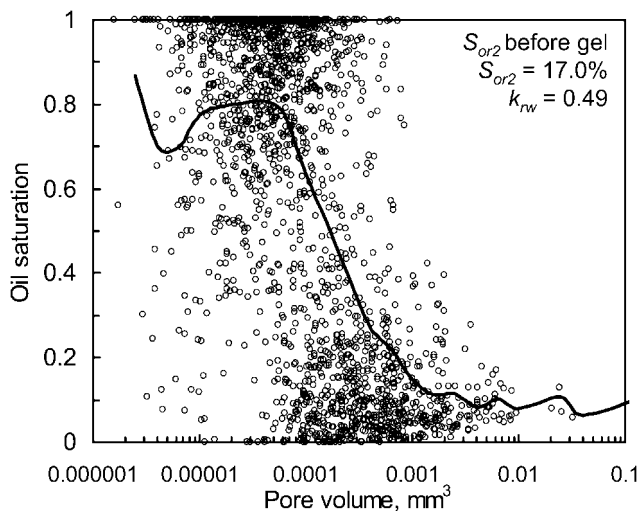


Fig. 7—Polyethylene at S_{or2} before gel.

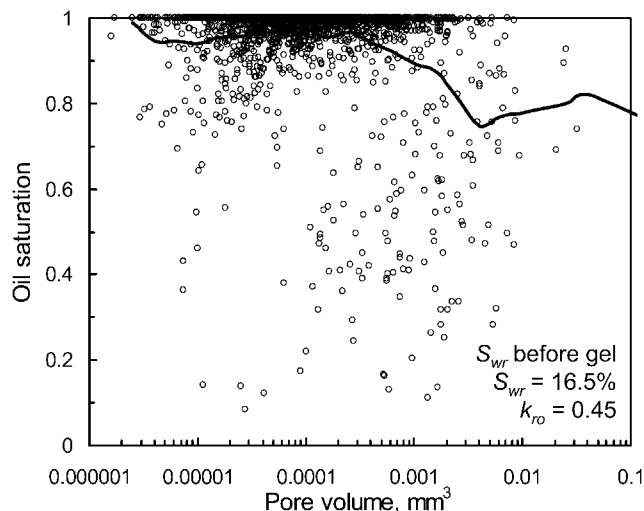


Fig. 8—Polyethylene at S_{wr} before gel.

when water was injected into porous polyethylene, oil usually became hydraulically isolated in the smallest detected pores because any remaining wetting film was too thin to efficiently drain oil. Consequently, high oil saturations were usually seen in the smallest detected polyethylene pores (Figs. 6 and 7).

Water Imbibition Into Berea: Saturation Changes Were Insensitive to Berea Pore Size. Water saturation at S_{or} in the imaged region in Berea was 81.6% (Table 2). The average pore saturation was not sensitive to pore size (solid curve in Fig. 10). For all size ranges, note the large number of pores with high water saturations; 39.4% of the pores had $S_{wi} > 95\%$. During the transition from S_{wr} to S_{or} in Berea (Fig. 11, and compare Figs. 9 and 10), pores in all detected size ranges experienced significant gains in water saturation (averaging 65.6%). Pore size did not appear to significantly influence the extent of the transition.

In Figs. 9 and 10, the solid curves suggest that the average water saturation in the largest pores was greater than in pores of intermediate size. However, this observation is probably an artifact resulting from the presence of very few large pores. The fortuitous saturations in the few large pores may have skewed the far-right portions of the curves in Figs. 9 and 10.

Connectivity of Phases Before Gel Placement. Analysis of the connectivity of the fluid phases produced results that were consistent with expectations and with previous work (Chatzis et al. 1983). Details can be found in Seright (2003a) and Seright et al.

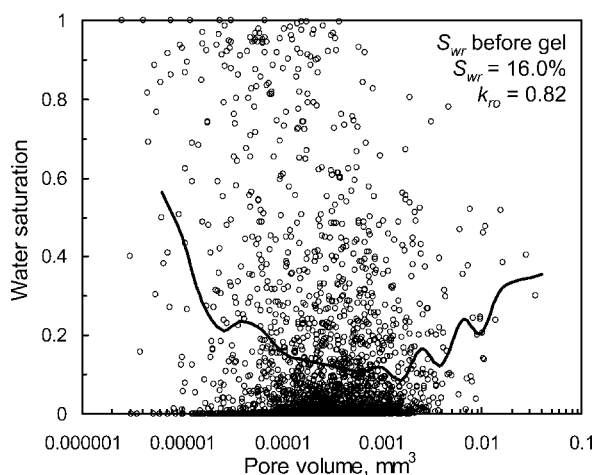


Fig. 9—Berea at S_{wr} before gel.

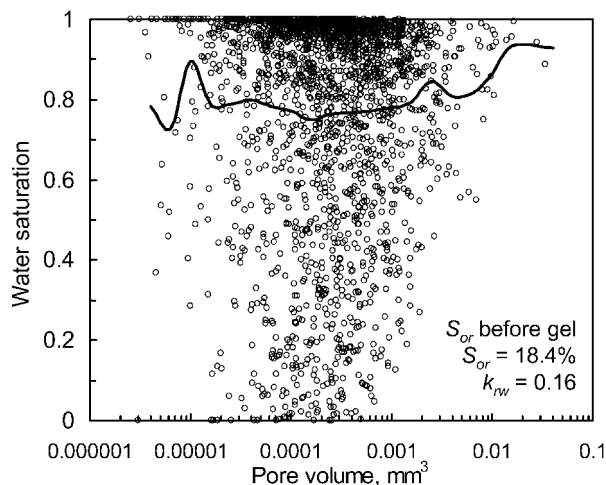


Fig. 10—Berea at S_{or} before gel.

(2004). A summary of findings (in both Berea and porous polyethylene) includes the following:

1. Before gel placement, at least 97.9% of the injected phase (oil or water) was connected.
2. Before gel placement, most residual nonwetting blobs were “singlets” (i.e., isolated within individual pores).
3. Changes in blob connectivity qualitatively followed the trends expected from the saturation changes. The largest oil blob always grew when the oil saturation increased and shrank when the oil saturation decreased. Similarly, the largest water blob always grew when the water saturation increased and shrank when the water saturation decreased.

Gelant Injection: 20-cp Gelant Mobilized Oil in Both Porous Media

During gelant placement in Berea, the oil saturation in the imaged region increased, surprisingly, from 18.4 to 36.3%. (In other words, water saturation decreased from 81.6 to 63.7% in Fig. 12.) To understand this result, note that the image volume was located in the center of the core and was small compared to the total pore volume of the core. Oil from upstream of the image volume was mobilized by flow of the 20-cp gelant, and that oil coincidentally lodged in the image volume. The overall oil saturation in the core did not change during gelant placement. (No oil was observed in the core effluent during gelant injection.) Within the imaged region, medium-to-large pores (10^{-4} to 10^{-2} mm³) were most likely to gain in oil saturation (Fig. 12). The pressure gradient during

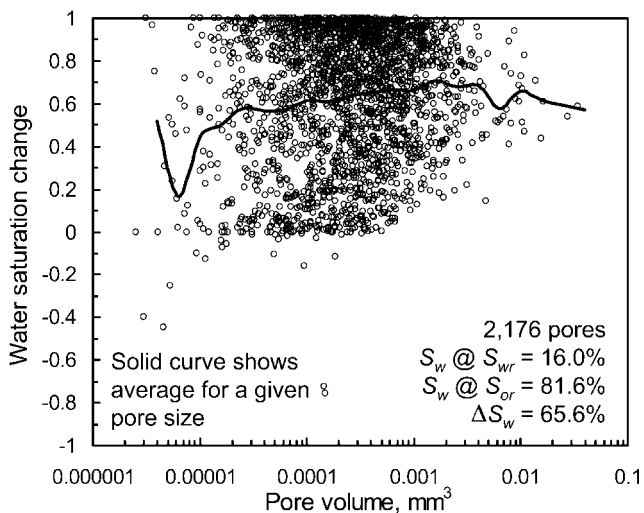


Fig. 11—Changes in Berea: S_{wr} to S_{or}

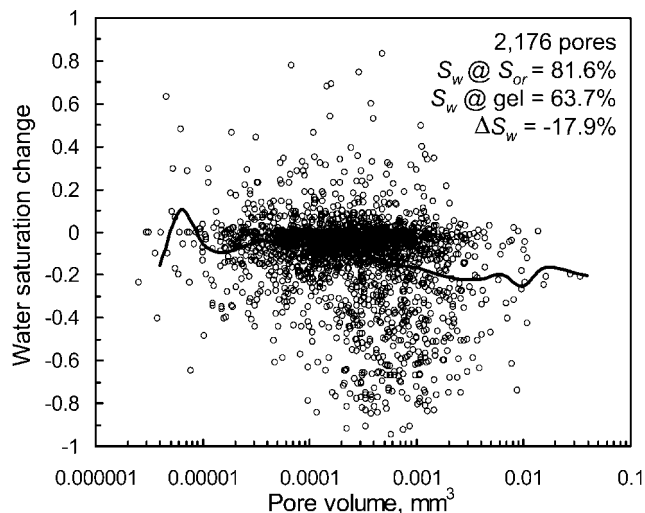


Fig. 12—Changes in Berea: S_{or} to gel placement.

gelant injection was always less than that during the previous brine or oil flows. This constraint was an intentional part of our experimental design to minimize oil mobilization. Because oil was mobilized, factors other than high pressure gradients were responsible for this mobilization.

During gelant placement in polyethylene, the gelant or aqueous saturation increased from 83 to 99.8% (Table 2). Most oil that was trapped in small pores was displaced, so that most pores ended with high gelant saturations (compare Figs. 7 and 13); only a few small pores retained large oil saturations (Fig. 13). As in Berea, the pressure gradient during gelant injection was always less than that during the previous brine or oil flows. Again, no oil was observed in the core effluent during gelant injection.

Why was oil mobilized from the small pores during gelant injection but not during the previous water injection—especially considering that the pressure gradient during water injection (35 psi/ft) was higher than that during gelant injection (23 psi/ft)? Could polymer or Cr(III) adsorption have altered the wettability (oil-wet to water-wet) of the polyethylene? This suggestion seems unlikely considering the hydrophobic nature of the surface and the hydrophilic nature of the polymer and crosslinker. Wang et al. (2001) suggested that viscoelastic forces associated with flow of polymer solutions may redistribute forces on a microscopic scale so that oil may be mobilized. This explanation may also help explain oil mobilization during our Berea experiments.

When gelant was placed, it effectively displaced all brine so that gel formed in all aqueous pore spaces. By itself, XMT cannot

distinguish between water and gel. However, this observation has been confirmed many times in previous work by noting that the Cr(III)-acetate-HPAM gel reduced permeability to water (for both Berea and polyethylene) to levels associated with the permeability of the gel itself to water (i.e., final permeability in the microdarcy range) (Seright 1999; Seright 1993).

Oil- and Waterflooding After Gel Placement

The imbibition and drainage displacements performed after gel placement address the primary goal of this work—to establish the mechanism for disproportionate permeability reduction for Cr(III)-acetate-HPAM gels. The most important conclusion from our earlier work was that oil injection effectively reduced gel volume (e.g., by dehydration) in many pathways that were used by oil before gel placement (Seright et al. 2002; Seright et al. 2004; Seright et al. 2003). This conclusion was confirmed in the present work. We define gel “dehydration” as a process of removing water from the gel by imposing a pressure gradient on the gel. Necessarily, the polymer must become more concentrated by the dehydration process, and its volume reduced.

Water Drainage From Berea: Oil Injection Reduced Gel Volume. During oil injection after gel formation, oil saturation increased by 35% (Table 2). Fig. 14 shows that most (95.2% of the total) pores gained oil (lost water) when oil was injected after gel placement. Oil effects on the gel were insensitive to pore size. Average water saturation (solid curve in Fig. 14) decreased by

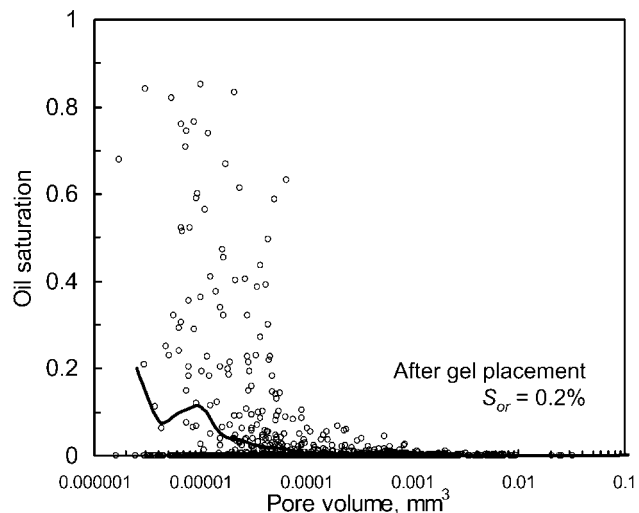


Fig. 13—Polyethylene after gel placement.

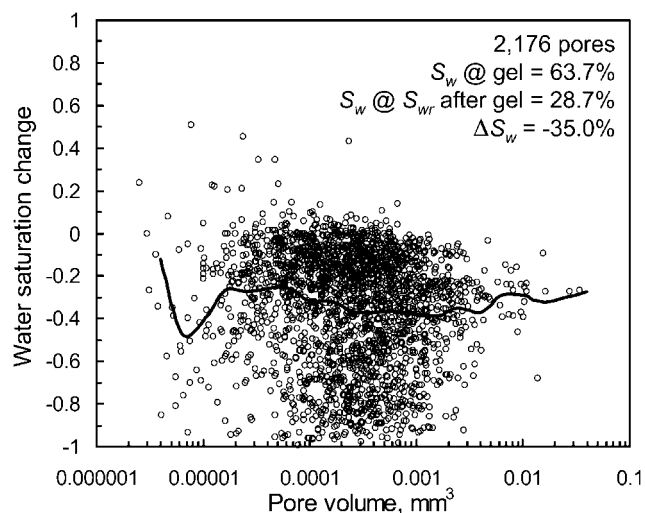


Fig. 14—Oilflooding to S_{wr} after gel placement in Berea.

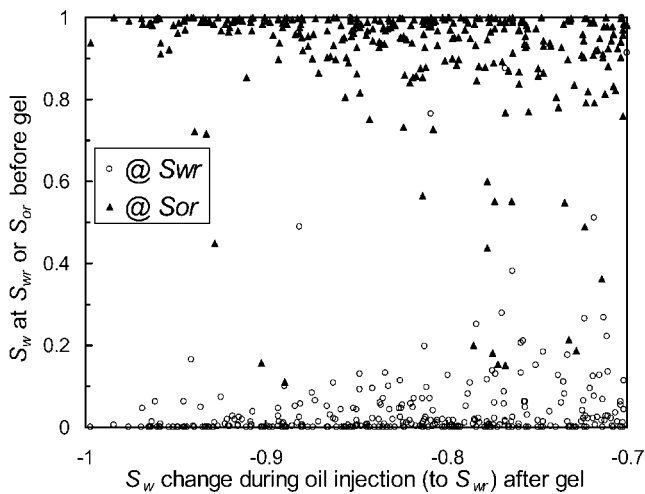


Fig. 15—Oil reduced gel volume most in pores that were easily filled by oil or water before gel. (300 of the 2,176 total pores.)

~35% regardless of pore size. Assuming that gel occupied all of the aqueous pore space, the oil apparently reduced the volume of the gel by 55% (water saturation was 63.7% immediately before, and 28.7% after, oil injection). The pressure gradients during these experiments were limited so that they never exceeded those applied before the gel was placed. Therefore, it seems unlikely that reduction in gel volume occurred because of exposure to excessive pressure gradients (i.e., extrusion of the gel from the core).

Fig. 15 provides additional insight into the process of gel volume reduction during oil injection. This plot shows the 300 pores (1/7 of total) that experienced the greatest increase in oil saturation (decrease in water saturation) during the process of oil injection after gel placement. Before gel placement, these pores were nearly full of oil at S_{wr} and were nearly full of water at S_{or} . Thus, oil and water both flowed freely into and filled these pores before gel placement. They were also easily accessible to oil after gel.

Water Drainage From Berea: S_{wr} in Berea Was Higher After Gel Placement Than Before. Overall residual water saturation was higher at S_{wr} after gel placement (28.7%) than before gel placement (16.0%). (See Table 2 and Fig. 16.) From Fig. 16, 86.1% of the pores had higher S_{wr} values after gel placement than before gel. Presumably, gel accounted for this increase—the gel is immobile but dehydrateable. In the previous section, we estimated that oil injection reduced gel volume by 55%. Fig. 16 suggests that the remaining gel was widely distributed, although it was most likely to be found in medium-to-small pores. Fig. 16 also shows

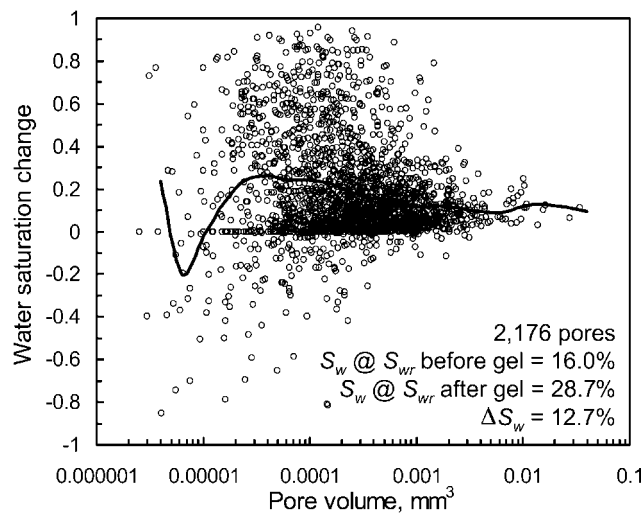


Fig. 16—Changes in Berea: S_{wr} before gel to S_{wr} after gel.

that a few pores had lower S_{wr} values after gel placement than before gel.

Water Imbibition Into Berea: Oil Was Trapped. During water imbibition after gel placement, the average increase in S_w was 20.3%—much smaller than the 65.6% average change that occurred before gel injection (Fig. 11). As was the case before gel injection, Fig. 17 reveals that a wide range of changes occurred for most pore sizes. The average saturation change was not particularly sensitive to pore size (although the average saturation changes were close to zero for the smaller pores). In contrast to the results before gel injection, 22.6% of the pores gained oil even though water was injected. Evidently, a significant degree of rearrangement occurred for water and oil saturations during imbibition after gel placement.

Commensurate with this, Fig. 18 reveals that at S_{or} after gel placement, 93.3% of the pores had higher oil saturations than at S_{or} before gel placement. Again, a wide range of changes occurred for all pore sizes, and the average change was not sensitive to pore size.

Residual Resistance Factors for Berea. The measured residual resistance factors were 15 for F_{rro} and 1,220 for F_{rrw} . Thus, gel presence reduced permeability to water 81 times more than to oil. As mentioned earlier, much of the gel was reduced in volume during oil injection after gel placement. Why was the final permeability to water so much lower than that to oil? Previous analysis (Seright et al. 2002; Seright et al. 2003) indicated that the gel

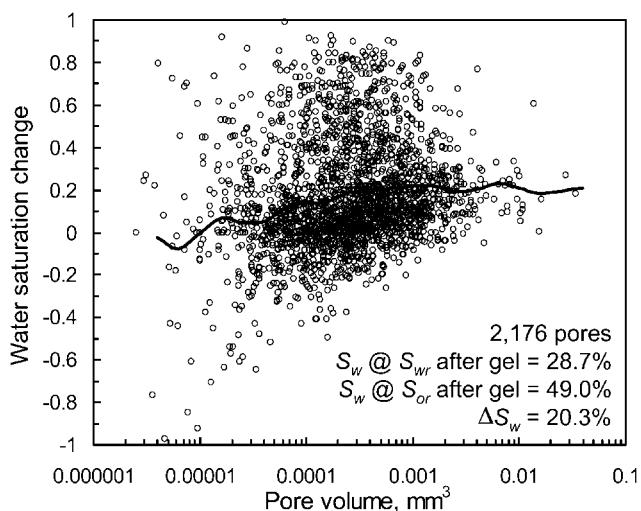


Fig. 17—Changes in Berea: S_{wr} after gel to S_{or} after gel.

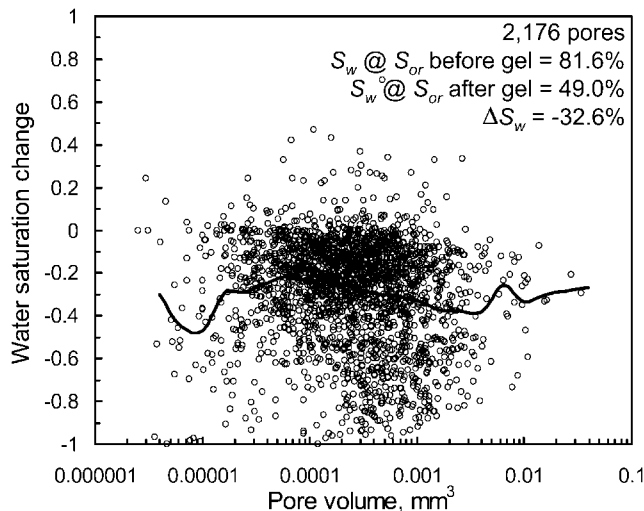


Fig. 18—Changes in Berea: S_{or} before gel to S_{or} after gel.

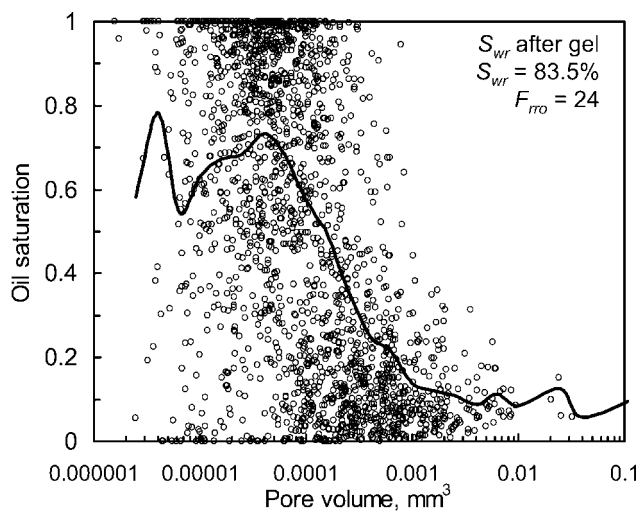


Fig. 19—Polyethylene at S_{wr} after gel.

trapped significantly more residual oil. Our new analysis, in which S_{or} jumped from 18.4% before gel placement to 51% after gel placement (i.e., S_w decreased from 81.6 to 49%; see Table 2 and Fig. 18), confirmed this conclusion. With many pores permanently occupied by oil, water was forced to flow through narrow films and through the gel itself, explaining the large value for F_{rrw} . In contrast, oil pathways were reopened by the oil, so F_{rro} was much less.

Oil Imbibition Into Polyethylene: Reduction of Gel Volume Occurred Mainly in Small Pores. When oil was injected after gel placement in polyethylene, the overall S_{wr} value was 83.5% (Fig. 19). For comparison, the overall S_{wr} value was only 16.5% before gel placement (Fig. 8). Presumably, the 67% difference was because of gel that was not dehydrated during oil injection. Put another way, oil injection reduced the gel volume by 16.3% (99.8 to 83.5%)—a reduction that was substantially less than that seen in Berea (35% from Table 2). If the reductions are attributed entirely to gel dehydration, the gel would have been concentrated by factors of 2.2 in Berea (i.e., 63.7/28.7) and only 1.2 in polyethylene (i.e., 99.8/83.5).

The oil saturation increased 63% for pores that were smaller than 10^{-4} mm³ but only by 11% for pores that were larger than 10^{-3} mm³ (see Fig. 20). Thus, compared to Berea, reduction of gel volume during oil injection into gel-filled porous polyethylene was more likely in small pores and less likely in large pores. If the

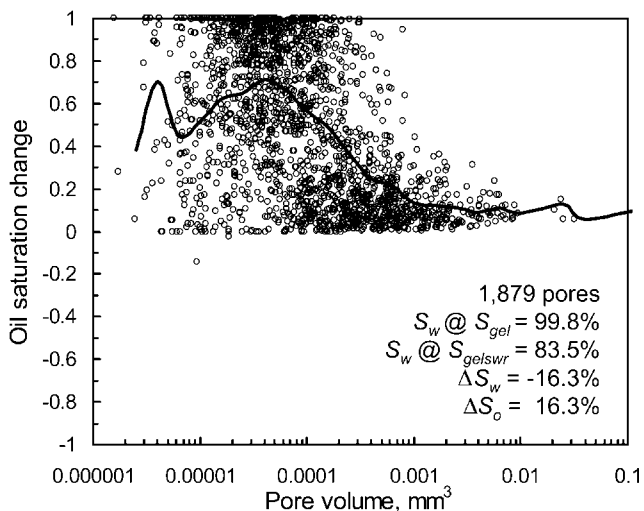


Fig. 20—Oilflooding to S_{wr} after gel placement in polyethylene.

losses are attributed to gel dehydration, the gel would have been concentrated by factors of 2.8 in small polyethylene pores and 1.1 in large polyethylene pores. Pressure gradients were not allowed to exceed 35 psi/ft during any stage of the polyethylene experiments. Therefore, it seems unlikely that reduction of gel volume occurred because of exposure to excessive pressure gradients. If high pressure gradients were responsible, gel damage should have been greater in larger pores than in smaller pores.

In Polyethylene, S_{wr} After Gel Placement Looked Like S_{or} Before Placement. A comparison of Figs. 6, 7, and 19 shows strong similarity between the saturation distributions at S_{wr} after gel placement in polyethylene and those at S_{or} before gel placement. Why should this similarity occur? Before gel placement, residual oil preferentially located in films and small pores. Medium-to-large pores provided the path of least resistance during oil displacement. However, after gel placement, medium-to-large pores were filled with immobile gel—providing substantial flow resistance for both oil and water. During oil injection after gel placement, capillary forces favored imbibition of oil through films and small pores. When water was subsequently injected, these oil-filled films and small pores apparently provided an easier flow path for water than that through the gel in the medium-to-large pores. Nevertheless, it is interesting that water could displace oil from the small pores after gel placement but not before gel placement. Pressure gradients after gel placement were no greater than before gel placement.

Oil Drainage From Polyethylene: Additional Oil Was Not Trapped During Water Injection. Saturations for the final water injection are plotted in Fig. 21; notice the similarity to Fig. 13. At S_{or} before and after gel placement, very little oil (less than 0.3%) remained in the imaged region. The small oil saturation that was present generally existed in the smallest pores.

Residual Resistance Factors for Polyethylene. For polyethylene, the oil residual resistance factor (F_{rro}) was 24. The mobile oil flows through films and the smallest pores. One might have expected much higher resistance to flow for low oil saturations and such narrow flow paths. The measured value for F_{rrw} was 2,130. Based on the S_w changes, the primary flow path for water is expected to be through the previously open oil paths, especially if little or no residual oil blocks the paths. However, if this were the case, F_{rrw} should not be 89 times greater than F_{rro} . On the other hand, the high water residual resistance factor could be explained if the oil paths closed up. During oil injection, paths may open by partial dehydration of the gel. During subsequent water injection, the paths could partially close when the gel rehydrates.

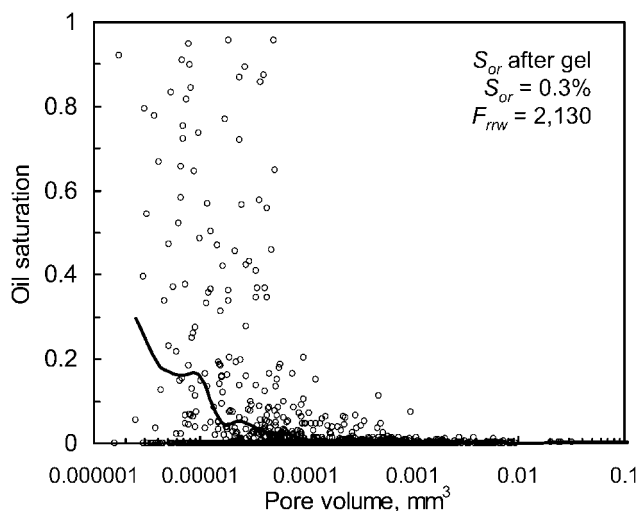


Fig. 21—Polyethylene at S_{or} after gel.

Connectivity of Phases After Gel Placement. During study of phase connectivity after gel placement, the most interesting observation was that in Berea the residual oil (resulting from water injection after gel placement) was highly connected. The S_{or} value was 51.0%, and 77.6% of that oil was contained within the largest oil blob. This blob was 122 times larger than the largest oil blob at S_{or} before gel placement. This high degree of connection helps explain the relatively high permeability to oil after gel placement. The largest blob was widespread, having occupancy in 73% of the pores in the image volume (1,588 out of 2,176 pores).

The pores that were involved with this largest oil blob had nearly the same distribution of pore sizes and water saturations as did all Berea pores in the image volume. For pores that participated with the largest oil blob, the average water saturation was 45%, compared with 49% for all Berea pores in the image volume.

Why should gel allow such a large oil blob to exist? Certainly, the oil phase was expected to be more connected for an S_{or} value of 51% than for 19.4%. Also, if oil was flowing within the porous media (at any fractional flow), the oil phase should be highly connected. However, at $S_{or}=51%$ after gel placement, *no* oil flowed, so this nonflowing oil phase *must* have existed as discrete blobs. The key question is: Why should the blob be so large?

We speculated that the gel located in the extremities of individual pores (i.e., near pore walls, especially in the vicinity of greatest pore radius) might reduce the effective pore radius to more closely match the effective throat radius. Thus, the effective pore-body/pore-throat aspect ratio could be reduced to allow residual oil to remain connected through multiple pores. (In other words, with a lower aspect ratio, residual oil drops would be less inclined to snap off and become trapped as “singlets” in individual pores, as occurs at S_{or} before gel placement.) This scenario is consistent with that suggested in Chatzis et al. (1983). To test this hypothesis, we analyzed the largest oil blob (at S_{or} after gel placement) as if it were a porous medium (i.e., with the oil representing the pore space, and everything outside the oil blob acting as “rock”). We found the “pore bodies” in the oil blob had a size distribution that closely paralleled the distribution for the original Berea sandstone.

The distributions of aspect ratios are compared in Fig. 22. Aspect ratio was defined as the effective pore radius divided by the effective throat radius. The effective pore radius was determined by assuming that the measured pore volume was spherical. The effective throat radius was determined by assuming that the measured throat area was circular. (In reality, although our pore volumes, throat areas, and shapes were known with reasonable accuracy, the pores were decidedly not spherical, and the throats were not circular.)

Contrary to our speculation, the gel did not reduce the effective pore-body/pore-throat aspect ratio. Instead, the average value (5.5)

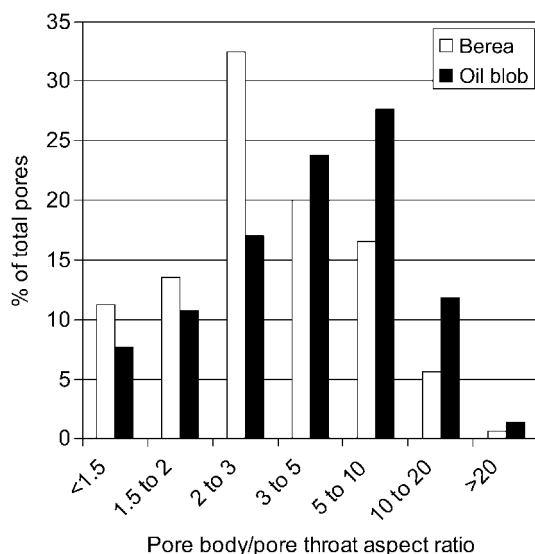


Fig. 22—Comparison of aspect ratios.

for the “aspect ratio” for the oil blob was 31% greater than that for Berea sandstone (4.2). For Berea pores, the peak in the distribution occurs at values from 2 to 3. In contrast, for the oil blob, the distribution peaked at values from 5 to 10.

The increase in aspect ratio associated with the presence of the gel might suggest that gel had a greater propensity to reside in pore throats than in pore bodies. However, the increased aspect ratio seems inconsistent with the existence of the large residual oil blob. With greater aspect ratios, why did the large oil blob not break up into many smaller blobs? A possible explanation is that water did not have access (or had limited access) to most of the pore throats after gel placement. With limited or no access, free water could not accumulate in pore throats to cause snap-off and form smaller oil blobs. The affinity of the gel to retain water could also explain why free-water films did not form and break up the largest oil blob.

The distribution of coordination numbers for Berea and the largest residual oil blob are compared in Fig. 23. Coordination number is the number of distinct exits from a given pore body. The average coordination number (3.6) for “pores” in the oil blob was 19% less than that for Berea sandstone (4.45). The peaks in the distributions occurred at a value of 3 in both cases. However, the oil blob had a much greater fraction of pores with low coordination numbers.

Mechanistic Implications

This section summarizes our current views of the mechanism for disproportionate permeability reduction for relatively “strong” (pore-filling) gels such as Cr(III)-acetate-HPAM.

Water Injected First After Gel Placement. Immediately after placement and gelation, the water-based gel occupies all of the aqueous pore space. Residual oil may be trapped in pore centers in water-wet rock such as Berea (see the schematic in Fig. 24). In oil-wet porous media (e.g., porous polyethylene), low-mobility “residual oil” may coat pore walls. If water or brine is injected after gel placement, it must flow through the gel itself (Fig. 24). Because the inherent permeability to water is in the microdarcy range for flow through the gel, a very large permeability reduction is observed (Seright 1993). For rock with an initial permeability (before gel) of approximately one darcy, the water residual resistance factor can be greater than 10,000. Thus, the gel can greatly reduce flow from gel-invaded water zones.

Oil Injected First After Gel Placement. Oil is typically the first fluid that contacts the gel-treated region when a well is returned to production. We found that oil reduces the pore volume occupied

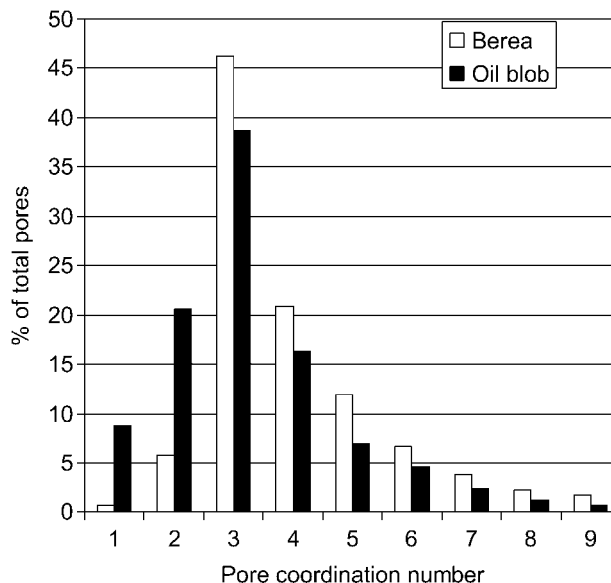
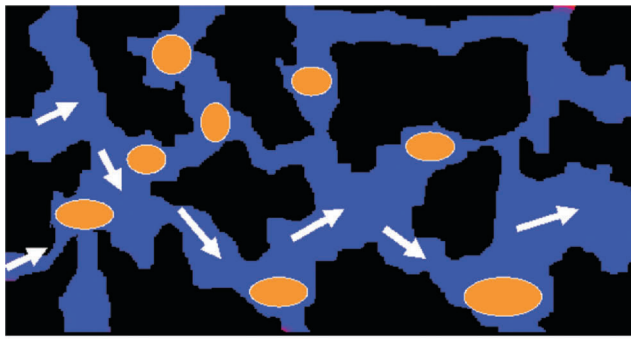


Fig. 23—Comparison of coordination numbers.



■ Immobile gel ■ Residual oil
 ➡ Water flow through gel

Fig. 24—Water must flow through the gel (Berea).

by gel. This volume reduction created pathways for oil flow, thus restoring an important level of permeability to oil. The schematic in Fig. 25 illustrates this process.

When oil is injected, how does a reduction in gel volume occur? Several possibilities come to mind, including oil (a) ripping through the gel, (b) concentrating or dehydrating the gel, (c) mobilizing the gel, or (d) chemically destroying the gel. As our oil (hexadecane) was not reactive with any of the gel, brine, or rock components, the possibility of chemical destruction of the gel does not seem likely. As we have never observed gel production from our cores, we view the possibility of gel mobilization as unlikely. However, it is possible that gel particles too small for us to detect were displaced from the core.

That leaves two mechanisms for active consideration. In one mechanism, oil ripped pathways through the gel (Seright et al. 2002; Seright et al. 2003; Al-Sharji et al. 1999; Zaitoun et al. 1998). In the second mechanism (Willhite et al. 2002; Ganguly et al. 2003; Nguyen et al. 2004), gel dehydrated.

Our recent analysis supports the dehydration mechanism over the ripping or gel-mobilization mechanisms. In particular, the apparent reduction in gel saturation during oil injection was insensitive to pore size in Berea (Fig. 14) and was greatest in small pores in porous polyethylene (Fig. 20). If ripping or gel mobilization were the dominant mechanisms, losses in gel volume should have been greatest in the largest pores. To explain, if gel failure (i.e., ripping or gel extrusion) occurred at a gel/rock interface or within the gel, force-balance analysis suggests that the pressure gradient for gel failure should be inversely proportional to the pore radius (Zaitoun et al. 1998; Liu and Seright 2001; Seright 2003b). Thus, for a given applied pressure gradient, gel failure should occur dominantly in larger pores. Because this did not occur, our results argue against the ripping or gel-mobilization mechanisms.

In contrast, the observed XMT results could be consistent with the dehydration mechanism. With a fixed pressure gradient applied through the porous medium, gel in all pores could be “squeezed” or dehydrated to the same extent, regardless of pore size.

Water Following Oil Flow After Gel Placement in Berea. If an oil zone that was treated with gel eventually waters out, our results

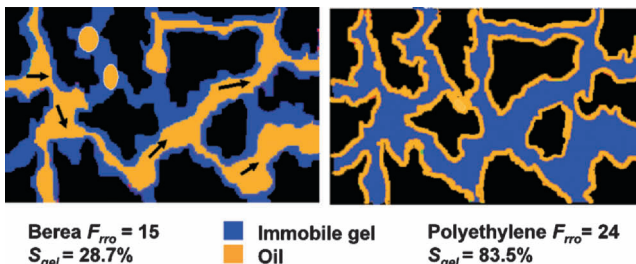


Fig. 25—Oil opens pathways by dehydrating the gel.

indicate that the water residual resistance factors will be substantially greater than the residual resistance factors observed during the previous oil flow. What mechanism can explain this behavior? In water-wet Berea sandstone, our results indicate that a significantly higher level of residual oil is trapped during water flow (Fig. 18 and Table 2). Even without the presence of gel, higher oil saturations necessarily lead to lower permeabilities to water. With higher oil saturations, water pathways would be more constricted. Given the large ratio of F_{rrw}/F_{rro} (81) in Berea, the primary pathways for water flow could conceivably be either thin water films and/or through the gel itself (see the schematic in Fig. 26).

When water was reinjected to establish S_{or} after gel placement, gels conceivably could rehydrate and swell to some extent. Did this occur? Table 2 indicates that the water saturation (or the combined water plus gel saturation) in Berea changed from 63.7% immediately after gel placement, to 28.7% at S_{wr} after gel, to 49% at S_{or} after gel. If the decrease in S_w from 63.7 to 28.7% during oil injection was the result of dehydration, the gel would have been concentrated by an average factor of 2.2. If the increase in S_w from 28.7 to 49% during water injection was entirely caused by rehydration, the gel would have swelled by a factor of 1.7.

Water Following Oil Flow After Gel Placement in Polyethylene. In contrast to the behavior in water-wet Berea, gel does not appear to trap high levels of residual oil during water flow following oil flow after gel placement (Table 2 and Fig. 21). Nevertheless, our results in polyethylene indicated that the water residual resistance factors were still substantially greater than the residual resistance factors observed during the previous oil flow ($F_{rrw}/F_{rro} = 89$). Similar to the case for Berea, the primary pathways for water flow could be either thin water films and/or through the gel itself (schematic in Fig. 27).

Table 2 indicates that the water saturation (or the combined water plus gel saturation) in polyethylene changed from 99.8% immediately after gel placement, to 83.5% at S_{wr} after gel, to 99.7% at S_{or} after gel. If the decrease in S_w from 99.8 to 83.5% during oil injection was entirely because of dehydration, the gel would have been concentrated by a factor of 1.2—much less than that observed in Berea. If the increase in S_w from 83.5 to 99.7% during water injection was entirely caused by rehydration, the gel would have swelled almost entirely back to its original size. Additional evidence of rehydration comes from the F_{rro} and F_{rrw} values for gel in the polyethylene core ($F_{rro} = 24$, $F_{rrw} = 2,130$). Because our earlier discussion suggested that oil and water may largely follow the same path, the high F_{rrw} value could be explained by gel rehydration partially closing the path.

Comparison With U. of Kansas Work

Researchers at the U. of Kansas advocated dehydration as the dominant mechanism for re-establishing oil pathways through the

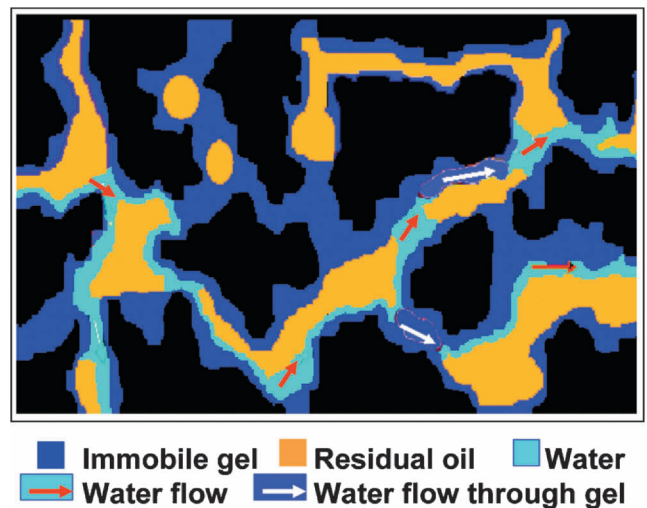


Fig. 26—Water flow following oil injection after gel placement in water-wet Berea.

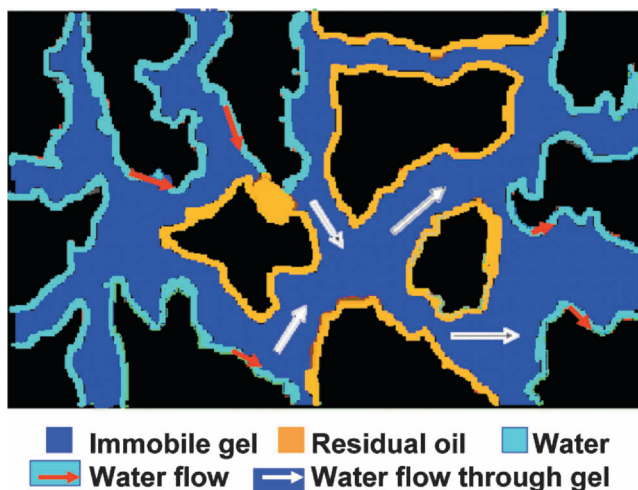


Fig. 27—Water flow following oil injection after gel placement in oil-wet polyethylene.

gel (Willhite et al. 2002; Ganguly et al. 2003; Nguyen et al. 2004). In recent work (Nguyen et al. 2004), they studied disproportionate permeability reduction provided by Cr(III)-acetate-HPAM gels in 4- to 5-darcy sandpacks. Using tracer studies with stilbene, they confirmed our finding of a high degree of connection for the oil phase (Seright et al. 2004; Liang et al. 1992). They also confirmed our finding that S_{or} in water-wet porous media was significantly higher after gel placement than before gel placement (Seright et al. 2002; Seright et al. 2004; Seright et al. 2003).

Although the U. of Kansas researchers argued in favor of a dehydration mechanism, confusion exists about their definition of “dehydration.” In addition to the definition that we accept (stated previously), Nguyen et al. (2004) contains at least two other definitions. A second definition [from Tables 4 through 6 in Nguyen et al. (2004)] is: [increase in oil saturation during oil injection after gel placement] relative to [gel saturation immediately after gel placement]. The third definition is that “dehydration” simply means oil injection.

In our view, a detailed analysis of their data (Seright 2004) indicates that ripping and gel-displacement mechanisms dominate over the dehydration mechanism. A key revelation from analysis of the data in Nguyen et al. (2004) was that a significant amount of polymer was produced with the effluent during oil injection. Typically, more than half the polymer was recovered. This indicated that a gel-destruction or -removal mechanism other than dehydration was very important. Thus, removal of polymer from the core played an important role in establishing oil pathways, and removal of this polymer was not directly tied to dehydration. Instead, gel destruction or removal might be caused by oil (1) ripping the gel apart so it was basically a polymer solution or (2) displacing gel from the core as very small particles (too small to detect).

To quantify the relative importance of dehydration vs. the destruction/displacement mechanism, consider experiment TN003 from Nguyen et al. (2004). The “fraction of gel dehydrated” was listed as 68.5%, and the fraction of polymer recovered was 45% [in Tables 4 and 5 of Nguyen et al. (2004)]. Oil injection created open space in the gel equivalent to 59.7% of the original pore space [87.1 to 27.4 from Table 8 of Nguyen et al. (2004)]. Recovery of 45% of the polymer suggests that 65.6% of the pore space that was opened by oil injection (i.e., $0.45 \times 87.1 / 59.7$) was actually caused by destruction or removal of the gel—not by dehydration. Performing these calculations for all cases in Nguyen et al. (2004) shows that destruction/removal of gel was more important than dehydration.

A close comparison of Tables 5 and 6 in Nguyen et al. (2004) indicates that raising the oil flooding pressure gradient from 20 to 50 psi/ft caused no apparent additional dehydration. [In all cases, the average remaining polymer concentration (in the core) decreased when the pressure gradient was increased from 20 to 50

psi/ft.] Consequently, only the gel-destruction/-removal mechanisms were significant.

In summary, the data in Nguyen et al. (2004) supports ripping or gel-displacement mechanisms over a dehydration mechanism. We note that the permeability of the sandpacks was from 4 to 5 darcys in the work at the U. of Kansas. In contrast, our Berea core had a permeability of 0.47 darcys. One would expect ripping or gel-displacement mechanisms to become more important as the permeability increases for water-wet porous media. Consequently, it is quite conceivable that the dehydration mechanism dominated in our 0.47-darcy Berea, while the ripping or gel-displacement mechanisms dominated in the sandpacks investigated at the U. of Kansas.

Conclusions

We used XMT to determine why a Cr(III)-acetate-HPAM gel reduces permeability to water more than that to oil in water-wet Berea sandstone and oil-wet porous polyethylene cores. The following conclusions were reached.

1. During the transition from S_{wr} to S_{or} in Berea before gel placement, pores in all detected size ranges experienced significant gains in water saturation. Pore size did not significantly influence the extent of the transition.

2. In contrast, in polyethylene before gel placement, oil was largely immobile in smaller pores.

3. Injection of 20-cp gelant mobilized oil in both porous media even though the pressure gradients during gelant placement were less than those during previous floods.

4. Immediately after gel placement, an extremely high resistance to water flow occurs (in either Berea or polyethylene) because impermeable gel occupies nearly all of the aqueous pore space.

5. During oil flow after gel placement in Berea, much of the gel was reduced in volume, leading to a relatively high permeability to oil.

6. At S_{or} after gel placement in Berea, 93.3% of the pores had higher oil saturations than at S_{or} before gel placement. The overall S_{or} in Berea jumped from 18.4% before gel placement to 51% after. The greater level of trapped oil greatly restricted water flow.

7. In polyethylene, reduction in gel volume occurred mainly in small pores.

8. The previously outlined observations suggest that reduction in gel volume in Berea sandstone and porous polyethylene was probably caused by a dehydration mechanism rather than a gel-ripping mechanism.

9. In contrast, data from other researchers support ripping or extrusion mechanisms for creating oil pathways in high-permeability sandpacks.

Nomenclature

F_{rro}	= oil residual resistance factor
F_{rrw}	= water residual resistance factor
k_{ro}	= relative permeability to oil
k_{rw}	= relative permeability to water
S_{gel}	= gel saturation
S_{or}	= residual oil saturation
S_{or1}	= first residual oil saturation before gel
S_{or2}	= second residual oil saturation before gel
S_w	= water saturation
S_{wr}	= connate or residual water saturation

Acknowledgments

Financial support for this work is gratefully acknowledged from the NPTO and NETL of the U.S. Dept. of Energy (DOE), the State of New Mexico, ExxonMobil, ConocoPhillips, Intevep/PDVSA, Marathon, Shell, and the Ufa branch of YuganskNIPIneft. We thank John Dunsmuir (ExxonMobil) for aid and use of the X2B beamline at Brookhaven Natl. Laboratory and Jenn-Tai Liang (U. of Kansas) and John Hagstrom for their part in collecting the XMT data. We thank Norman Morrow (U. of Wyoming), Jill Buckley, Robert Sydansk, and Julie Ruff for helpful technical discussions and thorough reviews of this paper. This research was carried out

(in part) at the Natl. Synchrotron Light Source, Brookhaven Natl. Laboratory, which is supported by the U.S. DOE, Div. of Materials Sciences and Div. of Chemical Sciences. The Geosciences Program of the U.S. DOE (Grant DE-FG02-92ER14261) funded development of the 3DMA-Rock code.

References

Al-Sharji, H.H., Grattoni, C.P., Dawe, R.A., and Zimmerman, R.W. 1999. Pore-Scale Study of the Flow of Oil and Water Through Polymer Gels. Paper SPE 56738 presented at the SPE Annual Technical Conference and Exhibition, Houston, 3–6 October.

Boneau, D.F. and Clampitt, R.L. 1977. A Surfactant System for the Oil-Wet Sandstone of the North Burbank Unit. *JPT* **29** (5): 501–506. SPE-5820-PA.

Chatzis, I., Morrow, N.R., and Lim, H.T. 1983. Magnitude and Detailed Structure of Residual Oil Saturation. *SPEJ* **23** (2): 311–326. SPE-10681-PA.

Dullien, F.A.L., Zarcone, C., Macdonald, I.F., Collins, A., and Borchard, R.D.E. 1989. The Effects of Surface Roughness on the Capillary Pressure Curves and the Heights of Capillary Rise in Glass Bead Packs. *J. Colloid Interf. Sci.* **127**: 362–372.

Dunsmuir, J.H., Ferguson, S.A., D’Amico, K.L., and Stokes, J.P. 1991. X-Ray Microtomography: A New Tool for the Characterization of Porous Media. Paper SPE 22860 presented at the SPE Annual Technical Conference and Exhibition, Dallas, 6–9 October.

Flannery, B.P., Deckman, H.W., Roberge, W.G., and D’Amico, K.C. 1987. Three-Dimensional X-Ray Microtomography. *Science* **237**: 1389.

Ganguly, S., Willhite, G.P., Green, D.W., and McCool, C.S. 2003. Effect of Flow Rate on Disproportionate Permeability Reduction. Paper SPE 80205 presented at the SPE International Symposium on Oilfield Chemistry, Houston, 5–7 February.

Liang, J., Sun, H., and Seright, R.S. 1992. Reduction of Oil and Water Permeabilities Using Gels. Paper SPE 24195 presented at the SPE/DOE Enhanced Oil Recovery Symposium, Tulsa, 22–24 April.

Lindquist, W.B. 3DMA-Rock: A Software Package for Automated Analysis of Rock Pore Structure in 3D Computed Microtomography Images. http://www.ams.sunysb.edu/~lindquis/3dma/3dma_rock/3dma_rock.html.

Lindquist, W.B. and Venkatarangan, A. 1999. Investigating 3D Geometry of Porous Media from High Resolution Images. *Phys. Chem. Earth (A)* **25**: 593–599.

Lindquist, W.B., Lee, S.M., Coker, D.A., Jones, K.W., and Spanne, P. 1996. Medial Axis Analysis of Void Structure in Three-Dimensional Tomographic Images of Porous Media. *J. Geophys. Res.* **101**: 8297–8310.

Lindquist, W.B., Venkatarangan, A., Dunsmuir, J., and Wong, T.-F. 2000. Pore and Throat Size Distributions Measured from Synchrotron X-Ray Tomographic Images on Fontainebleau Sandstones. *J. Geophys. Res.* **105**: 21508–21528.

Liu, J. and Seright, R.S. 2001. Rheology of Gels Used For Conformance Control in Fractures. *SPEJ* **6** (2): 120–125. SPE-70810-PA.

Nguyen, T.Q., Green, D.W., Willhite, G.P., and McCool, C.S. 2004. Effect of Composition of a Polyacrylamide-Chromium(III) Acetate Gel on the Magnitude of Gel Dehydration and Disproportionate Permeability Reduction. Paper SPE 89404 presented at the SPE/DOE Symposium on Improved Oil Recovery, Tulsa, 17–21 April.

Oh, W. and Lindquist, W.B. 1999. Image Thresholding by Indicator Kriging. *IEEE Trans. Pattern Anal. Mach. Intell.* **21**: 590–602.

Pitas, I. 1993. *Digital Image Processing Algorithms*. New York: Prentice Hall.

Prodanovic, M., Lindquist, W.B., and Seright, R.S. 2006 (submitted). Porous Structure and Fluid Partitioning in Polyethylene Cores from 3D X-Ray Microtomographic Imaging. *J. Colloid Interf. Sci.*

Seright, R.S. 1993. Effect of Rock Permeability on Gel Performance in Fluid-Diversion Applications. *In Situ* **17**: 363–386.

Seright, R.S. 1999. Using Chemicals to Optimize Conformance Control in Fractured Reservoirs. Annual Technical Progress Report (U.S. DOE Report DOE/BC/15110-2), U.S. DOE Contract DE-AC26-98BC15110, 21–28.

Seright, R.S. 2003a. Conformance Improvement Using Gels. Annual Technical Progress Report (U.S. DOE Report DOE/BC/15316-4), U.S. DOE Contract DE-FC26-01BC15316, 2–34.

Seright, R.S. 2003b. Washout of Cr(III)-Acetate-HPAM Gels From Fractures. Paper SPE 80200 presented at the SPE International Symposium on Oilfield Chemistry, Houston, 5–7 February.

Seright, R.S. 2004. Conformance Improvement Using Gels. Annual Technical Progress Report (U.S. DOE Report DOE/BC/15316-6), U.S. DOE Contract DE-FC26-01BC15316, 16–46.

Seright, R.S., Liang, J., Lindquist, W.B., and Dunsmuir, J.H. 2002. Characterizing Disproportionate Permeability Reduction Using Synchrotron X-Ray Computed Microtomography. *SPEJ* **5** (5): 355–364. SPE-79717-PA.

Seright, R.S., Liang, J., Lindquist, W.B., and Dunsmuir, J.H. 2003. Use of X-Ray Computed Microtomography to Understand Why Gels Reduce Permeability to Water More Than That to Oil. *J. Petro. Sci. Engin.* **39**: 217–230.

Seright, R.S., Prodanovic, M., and Lindquist, W.B. 2004. X-Ray Computed Microtomography Studies of Disproportionate Permeability Reduction. Paper SPE 89393 presented at the SPE/DOE Symposium on Improved Oil Recovery, Tulsa, 17–21 April.

Shin, S., Lindquist, W.B., Sahagian, D.L., and Song, S.-R. 2005. Analysis of the Vesicular Structure of Basalts. *Comput. & Geosci.* **31**: 473–487.

Wang, D., Huifen, X., Zhongchun, L., and Qingyan, Y. 2001. Study of the Mechanism of Polymer Solution with Visco-Elastic Behavior Increasing Microscopic Oil Displacement Efficiency and the Forming of Steady “Oil Thread” Flow Channels. Paper SPE 68723 presented at the SPE Asia Pacific Oil and Gas Conference and Exhibition, Jakarta, 17–19 April.

Willhite, G.P., Zhu, H., Natarajan, D., McCool, C.S., and Green, D.W. 2002. Mechanisms Causing Disproportionate Permeability in Porous Media Treated With Chromium Acetate/HPAAM Gels. *SPEJ* **7** (1): 100–108. SPE-77185-PA.

Zaitoun, A., Bertin, H., and Lasseux, D. 1998. Two-Phase Flow Property Modifications by Polymer Adsorption. Paper SPE 39631 presented at the SPE/DOE Improved Oil Recovery Symposium, Tulsa, 19–22 April.

SI Metric Conversion Factors

cp × 1.0*	E-03 = Pa·s
ft × 3.048*	E-01 = m
in. × 2.54*	E+00 = cm
md × 9.869 233	E-04 = μm ²
psi × 6.894 757	E+00 = kPa

*Conversions are exact.

Randy Seright is a Senior Engineer at the Petroleum Recovery Research Center of New Mexico Tech (Socorro). e-mail: randy@prcc.nmt.edu. He holds a BS degree in chemical engineering from Montana State U., Bozeman, and a PhD degree in chemical engineering from the U. of Wisconsin. **Masa Prodanovic** is a post-doctoral fellow at the Inst. for Computational Engineering and Sciences at the U. of Texas at Austin. e-mail: masha@ams.sunysb.edu. She holds a BS degree in applied mathematics from the U. of Zagreb, Croatia, and a PhD degree in computational applied mathematics from Stony Brook U. **Brent Lindquist** is a professor in the Dept. of Applied Mathematics and Statistics at Stony Brook U. e-mail: lindquis@ams.sunysb.edu. He holds a BS degree in physics from the U. of Manitoba and a PhD degree in physics from Cornell U.